ChemistryOpen

Minireviews
doi.org/10.1002/open.201900347

Chemistry Europe
European Chemical
Societies Publishing
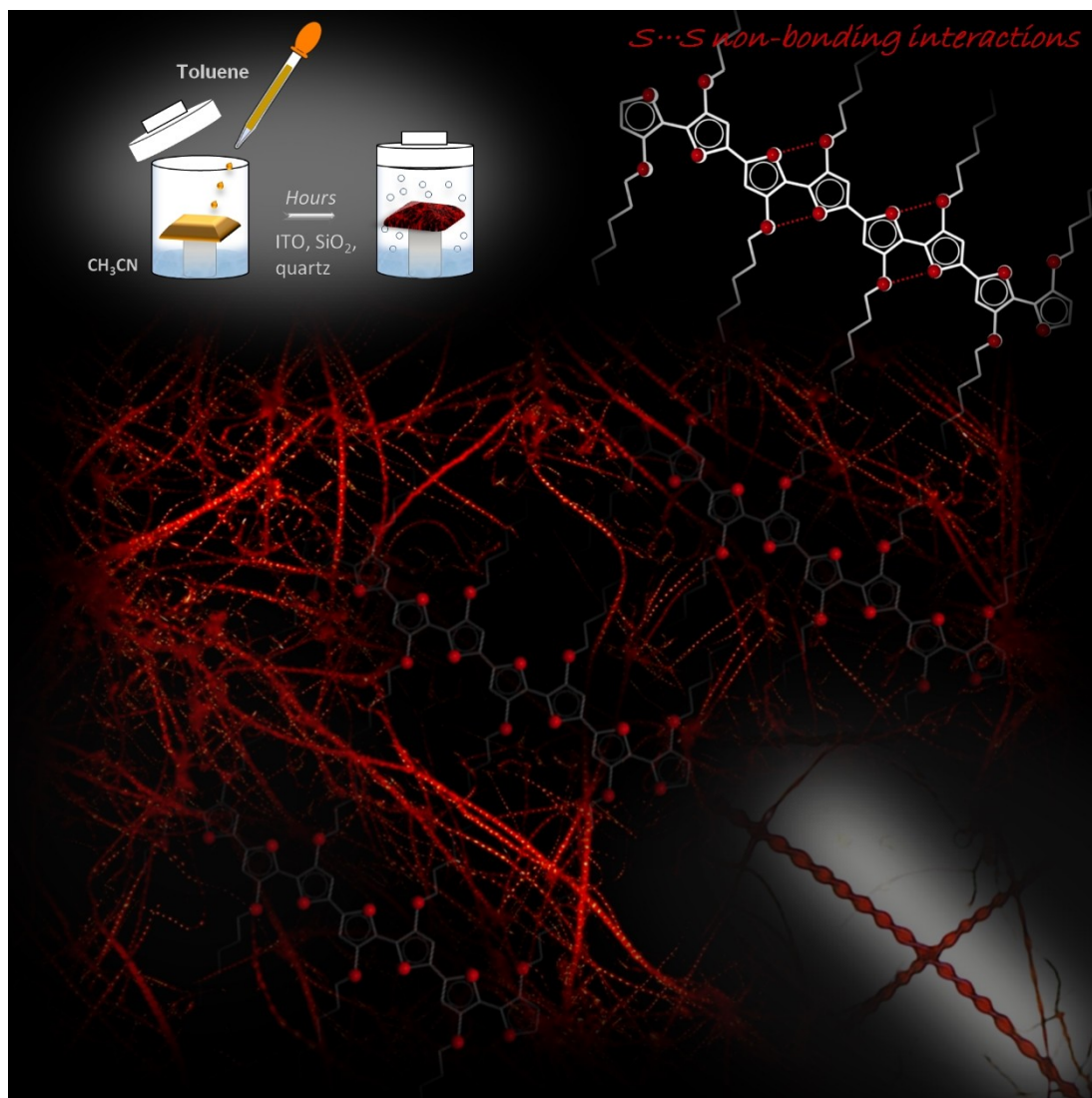
Supramolecular Assembly of Thiophene-Based Oligomers into Nanostructured Fluorescent Conductive and Chiral Microfibers

Mattia Zangoli,[b] Francesca Di Maria,*[a] and Giovanna Barbarella*[a, c]

The implementation of nano/microelectronic devices requires efficient strategies for the realization of supramolecular structures with desired function and supported on appropriate substrates. This article illustrates a strategy based on the synthesis of thiophene oligomers having the same "sulfur-overrich" quaterthiophene inner core (non bonding interactional algorithm) and different terminal groups. Nano/microfibers are formed on surfaces having a morphology independent of the nature of the deposition substrate and displaying a wide tuning of properties that make the fibers optoelectronically suitable for application in devices.

1. Introduction

Enabling specific properties and function of supramolecular structures by controlling the self-assembly of conjugated molecular building blocks is a main research object of bottom-up nano- and microtechnology.[1] Self-assembly and nanotechnology form the bases for materials and biosystems nanoarchitectonics.[2] Driven by weak noncovalent interactions with the surrounding environment, molecular materials and biosystems spontaneously assemble into hierarchical structures spanning multiple length scales and displaying different properties from those of the constituting units. Current research on semiconducting nano-microwires promises to revolutionize the field of integrated photonics,[3] while research on nanoparticles is expected to lead to dramatic improvements in nanomedicine and controlled drug delivery.[4] Owing to their numerous useful properties, from charge conduction to light emission, easy property tuning *via* organic synthesis and successful application in devices,[5] thiophene based oligomers and polymers are among the most studied building blocks to create functional supramolecular architectures by self-assembly.[1c,6] In particular, many studies have concerned poly(3-hexylthiophene-2,5-diyl), P3HT, one of the most appealing synthetic polymers with optoelectronic properties, employed in organic electronics, photovoltaics and more recently electrochromism.[7] Controlling the self-assembly of distinct building blocks requires the understanding of the relationship between molecular features and the noncovalent interactions directing the formation of the supramolecular structure: π–π stacking interactions, hydrogen bonding, hydrophilic/hydrophobic interactions, sulfur sulfur contacts, Van der Waals forces, metal interactions, and so forth.

Owing to its aromatic nature and planar backbone, thiophene displays a tendency to aggregation with other thiophenes or aromatic systems through π–π stacking interactions, also assisted by other noncovalent interactions. However, since the ring is geometrically deformable and adaptable[8] it is rather difficult to predict which ones of so many possible interactions are determining the final supramolecular architecture. Different chemical and physical strategies have been developed to govern the supramolecular assembly processes. One of the most reliable methods is to synthesize molecules in which one type of interaction is largely predominant, as in the case of barbiturated thiophene oligomers.[1c] However, predicting the supramolecular architectures resulting from specific ring substitutions is not always an easy task. For example, when polythiophene was functionalized with nucleotide complementary pairs in the hope of orienting the supramolecular growth *via* intermolecular W&C hydrogen bonds between complementary moieties, the results were completely different from expectations and, due to prevailing intra- and intermolecular thiophene-nucleobase stacking, puzzling crystalline microstructures were obtained.[9] In this article, we review the supramolecular organization of crystalline nano/microfibers promoted by a "sulfur-overrich" quaterthiophene building block, -T4S4-, containing one additional beta sulfur per ring. In its covalent network this structural element (3,3′,4′′,4′′′-tetrakis(hexylthio)-2,2′:5′,2′′′:5′′′,2′′′′:5′′′′,2′′′-quaterthiophene, which can be viewed as a "*non-bonding interactional algorithm*" according to Lenh's definition[10]), contains all the information needed to induce the directional and spontaneous self-assembly of X-T4S4-X oligomers into supramolecular fibers hierarchically organized from nano- to microscale. The synthesis of oligomers with different X groups allows the fine-tuning of the properties of the fibers, from morphology (rod-like or helical), to optical properties (all fibers are chiral at the nanoscale and fluorescent), to HOMO-LUMO energy gaps, to type of prevailing charge carriers (*p*- or *n*-type).

[a] Dr. F. Di Maria, Dr. G. Barbarella
     Istituto per la sintesi organica e fotoreattività (ISOF),
     Consiglio Nazionale delle Ricerche,Via Piero Gobetti, 101, 40129 Bologna,
     Italy
     E-mail: francesca.dimaria@isof.cnr.it
              giovanna.barbarella@isof.cnr.it
[b] Dr. M. Zangoli
     Istituto di Nanotecnologia (Nanotec),
     Consiglio Nazionale delle Ricerche, c/o Campus Ecotekne Università del
     Salento,
     via Monteroni, 73100 Lecce, Italy
[c] Dr. G. Barbarella
     Mediteknology srl,
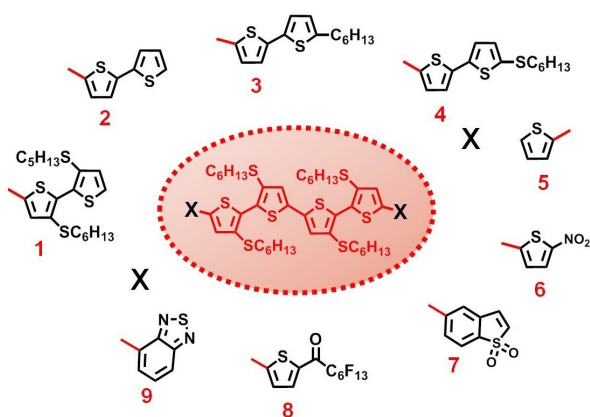   Via Piero Gobetti, 101, 40129 Bologna, Italy

2. Molecular Structures and Microfibers Preparation

The molecular structure of the thiophene based derivatives under review is shown in Scheme 1.

All compounds are characterized by the presence of the same inner "sulfur-overrich" quaterthiophene core, -T4S4-, having two head-to-head junctions of the thiohexyl side chains and different terminal X substituents. The name "sulfur-overrich" is due to the presence of an extra β sulfur atom for each

ChemistryOpen

Minireviews
doi.org/10.1002/open.201900347

Chemistry Europe
European Chemical
Societies Publishing

Scheme 1. Molecular structure of the thiophene-based oligomers reviewed in this article. In red the -T4S4-fragment.

thiophene ring compensating for the loss of π-conjugation due to inter-ring rotation originated by the steric effect of the substituents. Compounds **1–4** are octamers having the -T4S4-unit terminated by electron-rich alkylthio (SR) or alkyl (R) substituted 2,2′-bithiophene groups. Compound **5** is a hexamer terminated by unsubstituted thiophene rings, compounds **6** and **8** are hexamers terminated by thiophene rings bearing electron withdrawing groups, while **7** and **9** may be viewed as hexamers where the terminals are electron-poor fused rings. The synthesis of compounds **1–9** was carried out via Stille or Suzuki coupling, employing ultrasound for bromination and microwave irradiation for Suzuki cross-coupling reactions. All compounds were obtained in good yield and purity degree.[5b,11] We found that only the fragment -T4S4- promotes the formation of the microfibers, while different regiochemistry of the thiohexyl groups leads to amorphous morphologies.[12] Moreover, replacement of the hexyl chains with shorter alkyl chains causes the formation of star-shaped crystalline aggregates.[12] T4S4 terminated with H atoms does not form microfibers, while when bearing terminal aryl groups micro-

fibers are formed with rodlike or folded morphology depending on the terminals.[11] Figure 1 shows a sketch illustrating the formation of the microfibers on different surfaces. In the conditions indicated, at room T, compounds **1–9** are able to spontaneously self-assemble into polycrystalline nanostructured fibers via solvent exchange in solution.[13]

Compounds **1–9** were dissolved at room T in toluene and a few drops of the solution were deposited on the surface of choice placed on a solid support. Afterward the support was put inside a glass cylinder having acetonitrile at the bottom, a solvent in which **1–9** are poorly soluble. The molecules move slowly from toluene into acetonitrile, fast evaporation being inhibited. When acetonitrile vapors came in contact with the oligomer in toluene, crystallization in the form of randomly oriented microfibers took place. Then the substrate was removed and put on a Petri dish to dry. If not exposed to acetonitrile vapors, evaporation of the toluene solution only generated globular aggregates. The exposition time needed for fibers formation varied from a few minutes to hours depending on molecular structure. After exposition of a 10^{-3}–10^{-5} M toluene solution of **1–9** to acetonitrile vapors, the formation of fibers with high aspect ratio and characterized by micrometric length and width, and sub-micrometric thickness was observed (Figure 2, Figure 3). Microfibers formation was reproducible and led to the same morphology no matter whether glass, SiO_2, indium tin oxide (ITO) or gold were used as deposition substrates, indicating that the fibers were thermodynamically stable and their morphology was directed by the molecular structure. Generally, fibers made of oligothiophenes are rod-like and display morphology deeply affected by molecule-substrate interactions.[14] Clearly, in compounds **1–9** intermolecular interactions are prevailing so that the nano/microfibers can be directly grown on the desired substrate without needing mechanical transfer for integration into a device.[15]

Although the planar, electron-rich, -T4S4-fragment is crucial for fibers formation through π–π stacking, also the β-sulfur atoms play a key role in the hierarchical supramolecular organization process via intra- and intermolecular S···S

Giovanna Barbarella graduated at the University of Bologna (Italy) and received her Ph.D. in 1974 from the University of Grenoble (France). Currently, she is associate researcher at the Istituto per la Sintesi Organica e la Fotoreattività of the Italian National Research Council (ISOF-CNR). Her activity is focused on thiophene-based materials and their applications.

Francesca Di Maria graduated at the University of Catania (Italy) and received her Ph.D. in 2016 from the University of Bologna (Italy). She is currently a researcher at the Istituto per la Sintesi Organica e la Fotoreattività of the Italian National Research Council (ISOF-CNR). Her research interests are focused on the synthesis and characterization of thiophene-based materials and their organization into supramolecular nano- and microstructures.

Mattia Zangoli graduated at the University of Bologna (Italy) and received his Ph.D. in 2018 from the University of Bologna (Italy). He is currently a researcher at the Istituto per la Sintesi Organica e la Fotoreattività of the Italian National Research Council (ISOF-CNR). His research interests are focused on the synthesis of oligo- and polythiophens and their supramolecular organization into 0D and 1D structures.
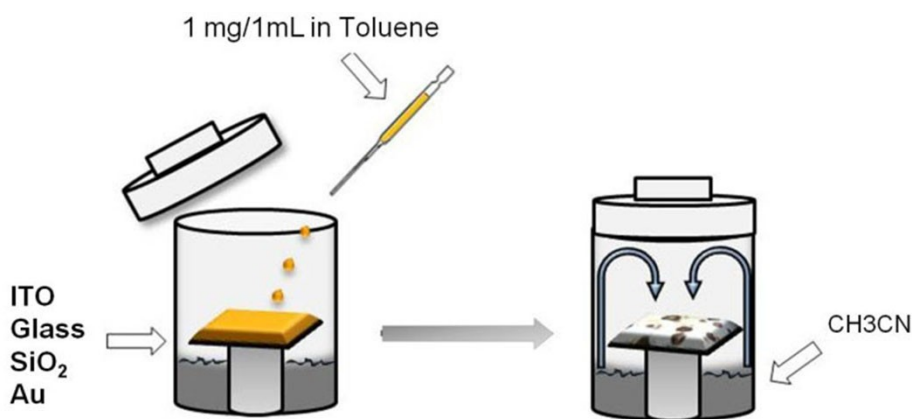
ChemistryOpen

Minireviews
doi.org/10.1002/open.201900347

**Chemistry
Europe**
European Chemical
Societies Publishing

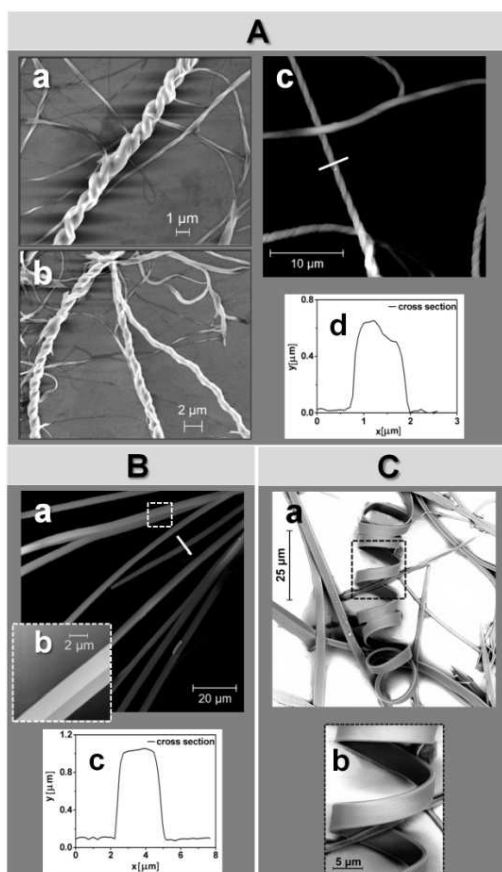**Figure 1.** Microfibers deposition by solvent exchange in solution.

Figure 2. (A) SEM (a and b on SiO_2), AFM (c, on glass) and AFM profile (d) of fibers of **1**; (B) AFM (a, on glass) and AFM profile (b) of fibers of **2**; (C) SEM (a and b on glass) images of fibers of **3**. Adapted with permission from reference [11a].

interactions.[16] Replacing the thiohexyl groups with hexyl groups generates amorphous aggregates in the same experimental conditions. The combination of the presence of thioalkyl groups, their head-to-head regiochemistry in the -T4S4-frag-

ment, and the S···S interactions define a building block storing in its covalent framework sufficient information to spontaneously promote the formation of well-defined supramolecular structures via nonbonded interactions. Optical microscopy showed that all fibers – helices as well as rod-like – displayed birefringence, extinguishing the transmitted light four times at intervals of 90° by rotating the plane of polarized light, indicating that they had a highly crystalline directional order. Supramolecular helicity was observed in all cases but **2**, **5** and **6**, which afforded rod-like instead of helical microfibers (Figures 2 and 3).

3. Optical Properties

3.1. UV/Vis and Fluorescence Spectra

The microfibers of **1**–**9** absorb in the range 400–700 nm (several nm red-shifted compared to the corresponding values in solution). They are intensely fluorescent in the range 600–850 nm, suggesting the formation of J-type (side-by-side) in place of H-type (face-to-face) aggregates.[11a] The similarity of the trend in fluorescence for all fibers suggests that they have similar supramolecular organisation at the nanoscale. Remarkably, the fibers from **8** and **6** with fluorescence maxima at 830 and 840 nm, respectively, show a broad emission spectrum extending up to 1200 nm (≈ 1.05 eV).

3.2. Circular Dichroism

All microfibers of both kinds, namely helical or rod-like, display circular dichroism (CD) signals in the range of the π–π transition observed in the UV/Vis spectrum of the corresponding oligomer, with signal intensities varying from a few mdegrees (θ) to 40–100 mdeg.[11,16] It is generally believed that only when stereocenters are present in the side chains it is
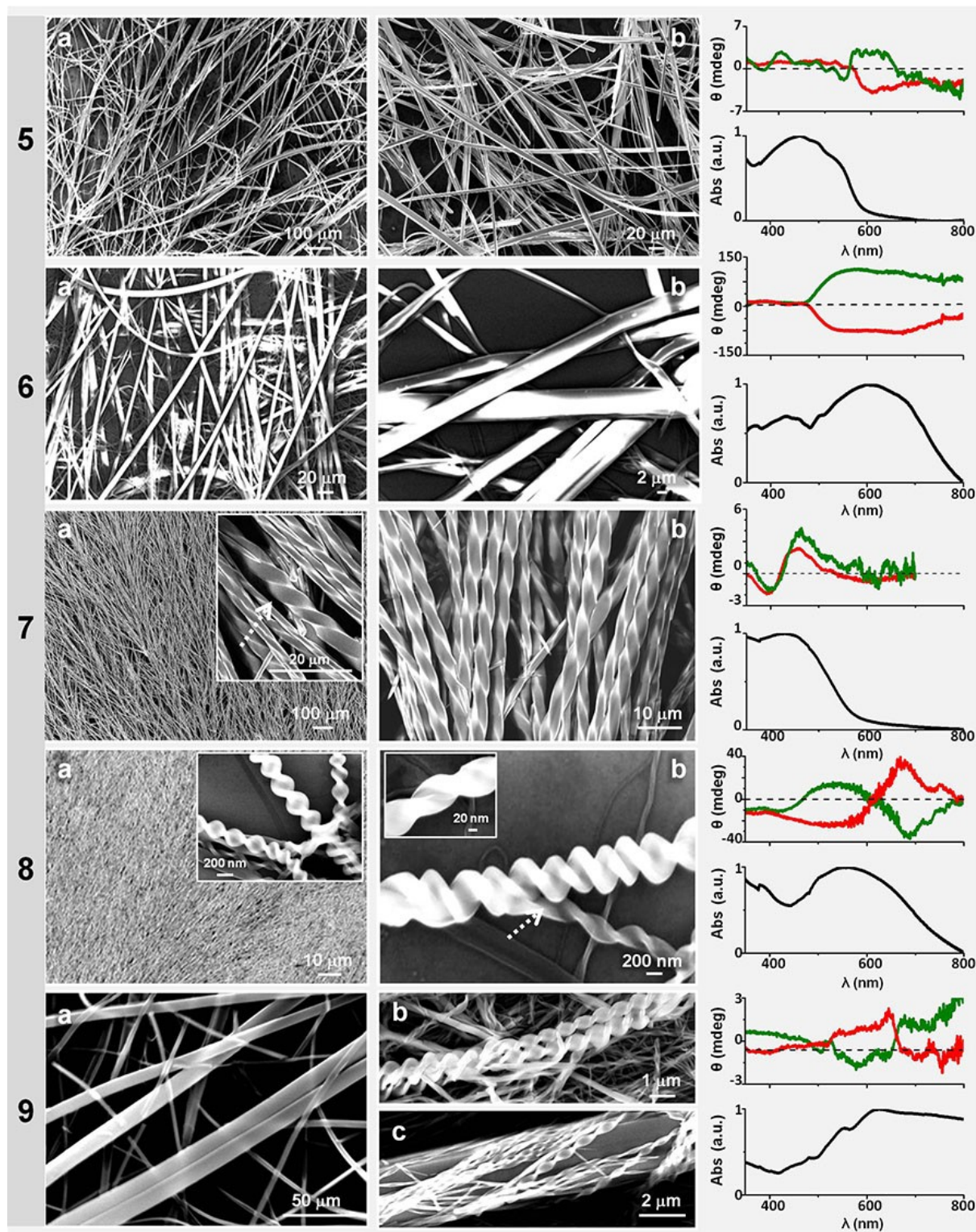
ChemistryOpen

Minireviews
doi.org/10.1002/open.201900347

Chemistry
Europe
European Chemical
Societies Publishing

Figure 3. SEM images of fibers of compounds **5** to **9** through the solvent-exchange method and circular dichroism (CD) plots of two different samples of the fibers of each compound. Adapted with permission from reference [11b].

possible to observe chirality in oligothiophene fibers.[17] As oligomers **1**–**9** do not have chiral substituents, the formation of helical or rod-like microfibers only depends on the molecular structure independently of the nature of the surface employed.

In solution, compounds **1**–**9** do not show CD signals being centrosymmetric molecules lacking chiral centers. In consequence, the CD signals of the microfibers arise from their supramolecular organization, causing adjacent chromophores

to interact and give rise to excitons within a nanometer scale range.[18] Factors capable of conferring chirality to **1–9** are molecular desymmetrization caused by distortions from planarity after deposition of the molecules on the substrate and/or the interactions between two molecules when they come in contact, being the latter factor supported by DFT calculations.[16] In both cases, the molecules acquire conformational chirality. Albeit the bias of one or more thiophene rings from the molecular plane is very small, chirality amplification[18,19] may take place during the assembly process leading to an observable CD signal. Since the bias of a tiophene ring (resulting in a change in the interring angle ω) takes place in one direction or the opposite ($+\omega$ or $-\omega$) with equal probability, thus CD signals displaying opposite Cotton effects can be expected in different points of the same sample or two different samples. In agreement with this, Figure 2 shows that the CD spectra of all compounds, with the esclusion of **7**, exhibit a Cotton effect of one sign and the opposite one corresponding to opposite helicity of the aggregates at the nanoscale. Despite repeated attempts, the fibers generated by compound **7** always displayed the same positive Cotton effect. Interestingly, the positive sign of the long-wavelength part of the CD signal of **7** reveals the presence of a right-handed helix at the nanoscale.[18] By contrast, the micrometer-sized double helices of superhelices observed in the SEM images of the supramolecular fibrillar structure of **7** shown in Figure 3 are indicative of left-handed helicity (M type) at the microscale. In consequence, the right-handed nanohelices self-assemble into left-handed superhelices at the microscale, as already observed for other types of fibers.[20] Supramolecular chirality is related to the packing type and, even if the chirality at the molecular level is the same, a different packing may lead to opposite supramolecular chiralities. The SEM images of microfibers of **8** (panel a, inset) and **9** (panel c) show the presence of nanoaggregates of opposite helicities. Also, the CD spectra of the rod-like microfibers of **5** and **6** indicate the presence of nanoaggregates of opposite helicities whereas at higher aggregation scales the helicity is lost due to molecular packing effects. Note that the rod-like microfibers of **6** show the largest CD intensity of all fibers.

4. Cyclic Voltammetry

The oxidation and reduction potentials of the microfibers, obtained by cyclic voltammetry (CV), were compared to those of the corresponding compounds in cast films and solutions.[11a,16] Notably, the reduction potential of the fibers was significantly less negative than that measured in solution and cast film for all compounds, indicating that upon self-assembly into fibers an increase in electron affinity is obtained. For example, compound **1** shows a reduction potential of −1.45 V in fibers, −1.58 V in cast film and −1.65 V in solution.[11a] Compound **5** in solution and cast film has a reduction wave at −1.8 V, i.e. outside the electrochemical window of the electrolyte, whereas the corresponding fibers show a reduction potential of −1.41 V.[16] Also compounds **6–9** display less negative reduction potentials in fibers compared to cast films

or solution. Consequently, passing from solution to fibers there is a significant decrease in the energy gap, the lowest energy gap being that of compound **6** (1.53 eV).

5. Charge Transport and Charge Carriers

The microfibers obtained from compounds **1–9** are all conductive and even photoconductive.[11] The possibility to reproducibly grow the microfibers with the same morphology on different substrates allowed investigations employing many techniques requiring deposition on glass, ITO, SiO_2, and gold. Moreover, to test the applicability in devices, the fibers were directly grown on the SiO_2 surface of a field-effect transistor with gold contacts to measure FET charge mobilities. The nanoscale charge conductivity of the microfibers of **1,2** directly grown on ITO was measured by conductive atomic force microscopy (C-AFM) and tunneling atomic force microscopy in torsion mode (Tr-TUNA),[11a] a scanning probe technique that simultaneously shows surface topography and local current and provides information on nanoscale conductivity within specific domains.[21] The results are shown in Figure 4 for the helical and rod-like microfibers obtained respectively from **1** and **2**. A direct correlation of Tr-TUNA images with the topography reveals defined conductive domains associated to the fibers. The charge mobility at the nanoscale of the fibers of **1** and **2** was obtained by conductive-AFM in contact mode (C-AFM). Both microfibers display p-type (hole-transporting) characteristics with charge mobility values, μ_{holes}, of 9.8×10^{-7} and 5×10^{-6} cm^2/Vs, respectively, in agreement with Tr-TUNA maps.

As soon as they are formed, the microfibers of **1–9** are randomly distributed on the different substrates used. Nevertheless, well-ordered aligned microfibers can be obtained by employing the lithographically controlled wetting (LCW)[22] technique in order to direct their self-organization in a confined environment. Figure 5 shows that in this way well-aligned microfibers are obtained displaying a substantial enhancement of charge mobility.[23]

Aligned microfibers obtained from compounds **2–4** exhibited charge mobility values increased by about 3 orders of magnitude compared to OFETs based on randomly distributed fibers and I_{on}/I_{off} values increased by approximately one order of magnitude.[23] The surface electronic potential of microfibers of **5–9** grown on glass were investigated by Kelvin Probe Force Microscopy (KPFM), a technique allowing to measure the work function of the fibers with respect to the gold tip value: $\varphi = \varphi fiber - \varphi Au$[24] (see scheme in Figure 6). Figure 6 shows the work function of the fibers of **5–9**. In agreement with previous characterizations,[25] two classes of fibers can be distinguished, those with work function value higher than gold ($\varphi-\varphi Au > 0$) indicative of an increase of hole density at surface (electrons moving from the fibers to the tip), corresponding to the fibers obtained from **5**, and those showing work function values lower than gold ($\varphi-\varphi Au < 0$) indicative of an increase of the electron density (electrons moving from the tip to the fiber) and corresponding to the fibers obtained from **6** to **9**. Consequently, the fibers of **1** are p-type whereas the fibers of **2–5** are n-type,

ChemistryOpen

Minireviews
doi.org/10.1002/open.201900347

Chemistry
Europe

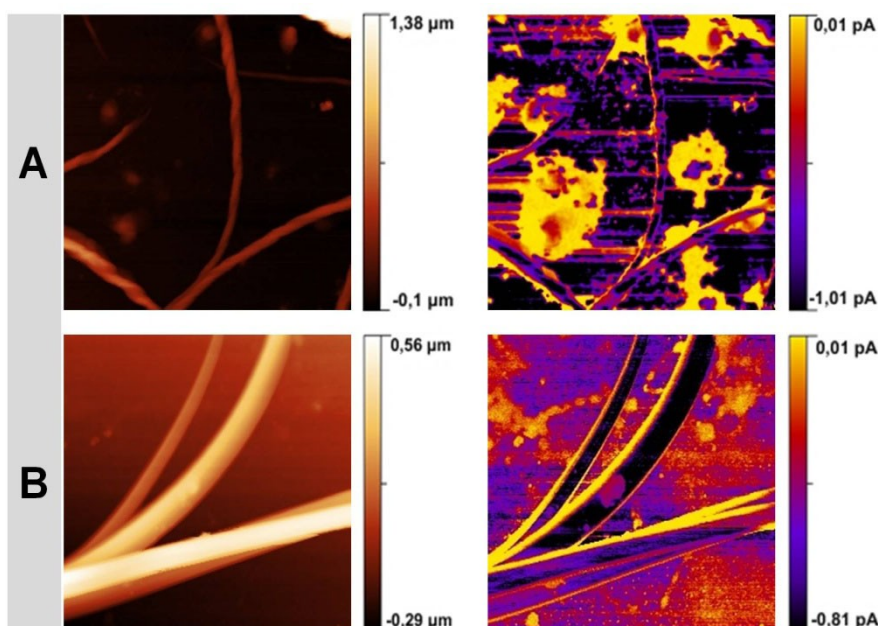European Chemical
Societies Publishing

Figure 4. (A) Topography image (left) and hole transportation measurement (right) of helical fibers of **1** grown on ITO obtained using Tr-TUNA with a 5 V bias on the tip. (B) The same as panel A for rod-like fibers of **2**. Adapted with permission from reference [11a].
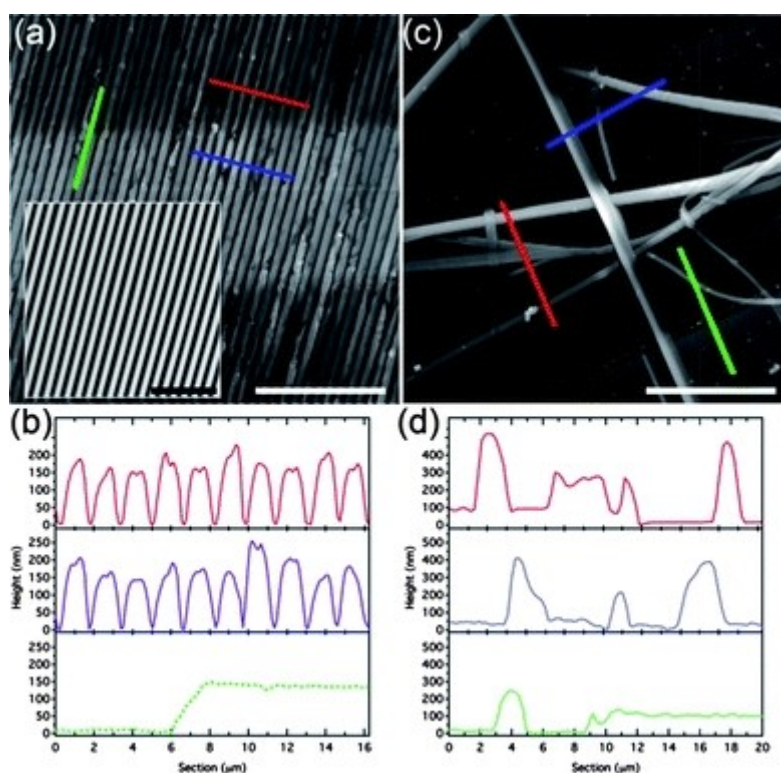

Figure 5. Typical AFM topography (scale bar $^1/_4$ 20 mm, z scale 0–250 nm), and corresponding profiles of (a and b) aligned and (c and d) randomly distributed fibers on an interdigitated electrode/SiO$_2$ surface (scale bar $^1/_4$ 20 mm, z scales (a) 0–250 nm, (b) 0–500 nm). The inset in (a) shows the AFM topography image of a PDMS stamp (scale bar $^1/_4$ 10 mm, z scale 0–250 nm). Here we have shown fibers of **2** (**3** and **4** exhibit a similar morphology). Reproduced with permission from reference [23].

i.e., the functionalization with strong electron acceptors groups determines the reverse of the sign of charge carriers. The results are in line with cyclovoltammetry data, indicating that passing from the fibers formed by **5** to those formed by **6**–**9** the electron affinity strongly increases.[11b] They are also in agreement with DFT calculations according to which changing the

ChemistryOpen

Minireviews
doi.org/10.1002/open.201900347

**Chemistry
Europe**
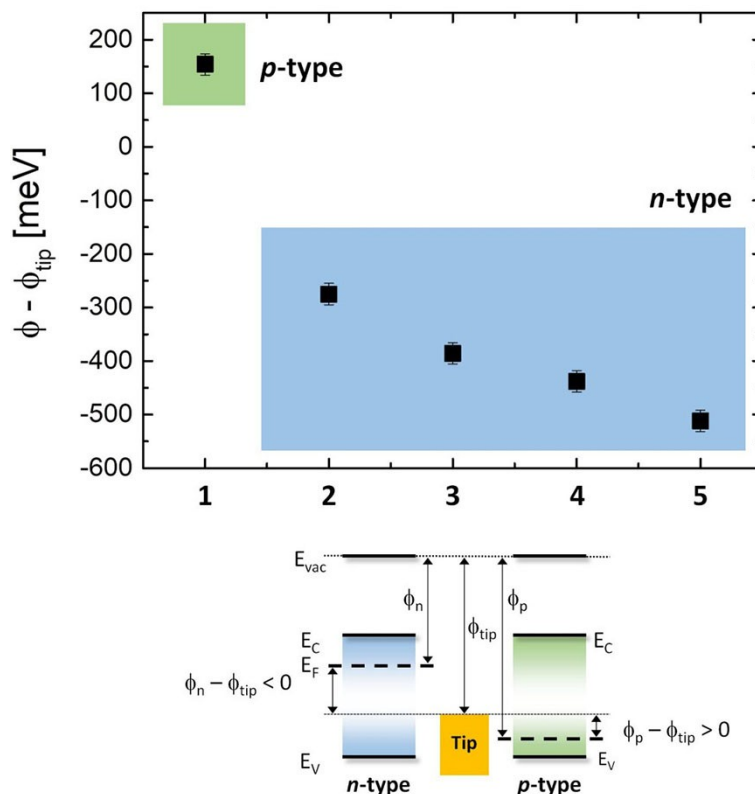European Chemical
Societies Publishing

Figure 6. Surface electronic potential measured by KPFM for the fibers of **5–9** grown on glass and energy diagram for *p*-type and *n*-type charge carriers. Reproduced with permission from reference [11b].

terminal groups causes a significant molecular charge redistribution.[11b]

6. Polymorphysm in Microfibers

Polymorphism has often been observed in thiophene derivatives, in particular conformational polymorphism in single crystals, where different conformations of the same molecule cause different packing modalities.[26] Conformational polymorphism and different packing modalities have early been detected for unsubstituted quater-[27] and sexithiophene.[28] More recently, we have reported the polymorphs of a thiomethyl substituted quaterthiophene[29] as well as of a tetramethyl substituted sexithiophene.[30] Conformational polymorphism between amorphous and crystalline phase is at the origin of the fabrication of a bicolored pixel structure LED based on a single luminescent oligothiophene.[31] Polymorphic needle-shaped crystals and crystalline nanofibers with very different functional properties and reproducibly grown on different substrates have also recently been reported.[32] We have described the first example of polymorphic microfibers generated from a 'sulphur overrich' octamer, namely 3,3',3''',3''''',3''''''',4'',4'''',4''''''-octakis (hexylsulphanyl), **1**.[16] This compound is synthesized in the form of red crystalline powder with traces of a further yellow crystalline powder. Upon empirical research we were able to increase the amount of yellow powder and found that it has

the same composition as the red one but with a different X-ray diffraction profile, as shown in panel A of Figure 7.

Both powders self-assemble spontaneously and reproducibly on surfaces of various types by solvent exchange at room temperature generating red and yellow fluorescent microfibers (top of panels B and C of Figure 7, respectively). While the red emitting microfibers are helical, i.e. display supramolecular chirality (see also Figure 2 showing the formation of superhelices, i.e. helices of helices), the supramolecular microfibers obtained from the yellow emitting powder are tape-like. Nevertheless, both types of microfibers display chirality at the nanoscale as shown by the corresponding CD spectra of panels B and C in Figure 7. The figure shows the CD spectra (reversed in sign) of two different samples of both types of fibers. The CD spectra of the red microfibers show enlarged bands compared to those of the yellow polymorph, which indicate the presence of supramolecular helicity.[33] It is worth noting that the yellow fibers are the first example reported so far of tape-like microfibers displaying a CD spectrum. Red and yellow microfibers were directly grown on the Si/SiO$_2$ substrate of a prefabricated bottom-gate, bottom-contact field effect transistor to measure their saturated charge mobilities and other electrical properties. Figure 7, panels B and C, show the AFM images and AFM profiles of the red and yellow fibers directly grown on FET devices, together with the corresponding electrical transfers in saturation regime.
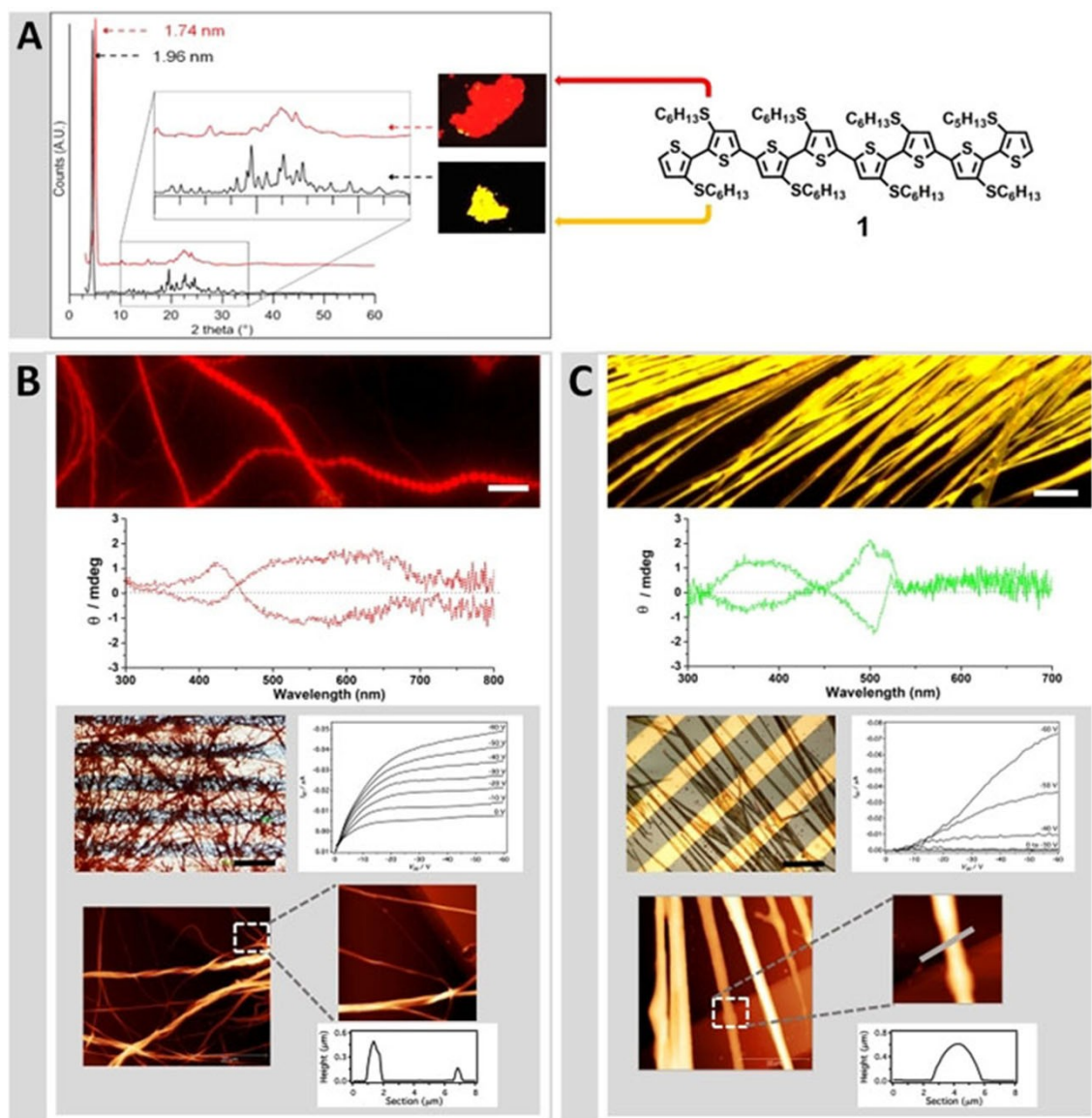
ChemistryOpen

Minireviews
doi.org/10.1002/open.201900347

Chemistry Europe
European Chemical
Societies Publishing

Figure 7. A) Plots of X-ray analysis of the microcrystalline powders of compound **1**. The insets are microscopy fluorescence images of the red and yellow powders. B) From top down: fluorescence image and circular dichroism spectra of two different samples of the red microfibers deposited on glass; AFM and AFM profile of the red microfibers directly grown on a FET device, together with the corresponding electrical transfers in saturation regime. C) The same for the yellow microfibers. Adapted with permission from reference [16].

The AFM images display that the yellow microfibers are characterized by tape-like morphology and the red ones by helical morphology with nearly the same submicrometric thickness. Both types of fibers show *p*-type charge transport features. However, the device with the yellow microfibers shows one order of magnitude higher field-effect charge mobility, μ_{sat}, and three orders of magnitude larger Ion/Ioff ratio than that with red ones. Since the yellow and red fibers are polymorphic supramolecular structures, the different electrical properties must be related to molecular packing, favouring the charge transport in the yellow polymorph.[16] This is in agreement with X-ray diffraction data indicating that the interlayer distance in the yellow phase is smaller than in the red one. Moreover, the yellow phase has a higher tendency to form more ordered

crystalline domains, allowing better orbitals overlapping hence more efficient electron transfer.

7. Main Non-Bonding Interactions

Powder X-ray diffraction studies and density functional theory (DFT) calculations on single molecules and their dimers afforded information useful to understand the main non-bonding interactions causing the formation of the microfibers.[11] The X-ray diffraction plots of all fiber samples displayed patterns with sharp and well separated peaks, flat background and the presence of second-order reflections, indicative of highly crystalline materials. The calculated non-covalent interaction

ChemistryOpen

Minireviews
doi.org/10.1002/open.201900347

Chemistry Europe
European Chemical
Societies Publishing

(NCI) indicator, capable of identifying hydrogen bonding regions in real space[34] was employed to highlight the interactions in the dimers of **5**–**9**. In agreement with our expectations, we found that the major role was played by π–π* stacking interaction between the molecular backbones. However, additional interactions such as hydrogen bondings (as in compounds **6,7**), became important when varying the terminal groups. Figure 8 illustrates two extreme cases, those of sexithiophenes **5** and **8**. In the former compound, the π–π* stacking is by far the main force binding the two interacting molecules. By contrast, in compound **8** the presence of fluorinated alkyl chains involves a significant depletion of charge in the π system of the molecular backbone and accumulation on the fluorine atoms. In consequence, in the dimer only a very small π–π* stacking interaction is observed accompanied by a significant interaction between the fluorine atoms of one molecule and the backbone of the other molecule. For compounds **6,7** the NCI indicator shows hydrogen bond regions between the oxygen atoms and the hydrogens or the backbone. Owing to the different position of the

oxygen atoms, which are in plane in **6** and out of plane in **7**, the structures of the dimers are different. Hydrogen bonding interactions involving the hexyl groups are observed for **6**, cause the twisting of the two molecules around each other without significantly distorting the backbone. On the contrary, in **7** the oxygen atoms do not interact with the hydrogens of the hexyls but with the molecular backbone causing a strong distortion of the backbone of each individual molecule.[11b]

8. Proposed Molecular Self-Assembly and Packing Mechanism

Based on small angle X-ray diffraction data obtained from the fibers of octamers **1**–**4** and taking into account all fibers' properties, in particular their intense fluorescence, we assumed that the octamers had a nearly planar backbone with almost perpendicular subtituents and were J-stacked in parallel rows forming a lamellar structure as displayed in Figure 9A.[11a] Single
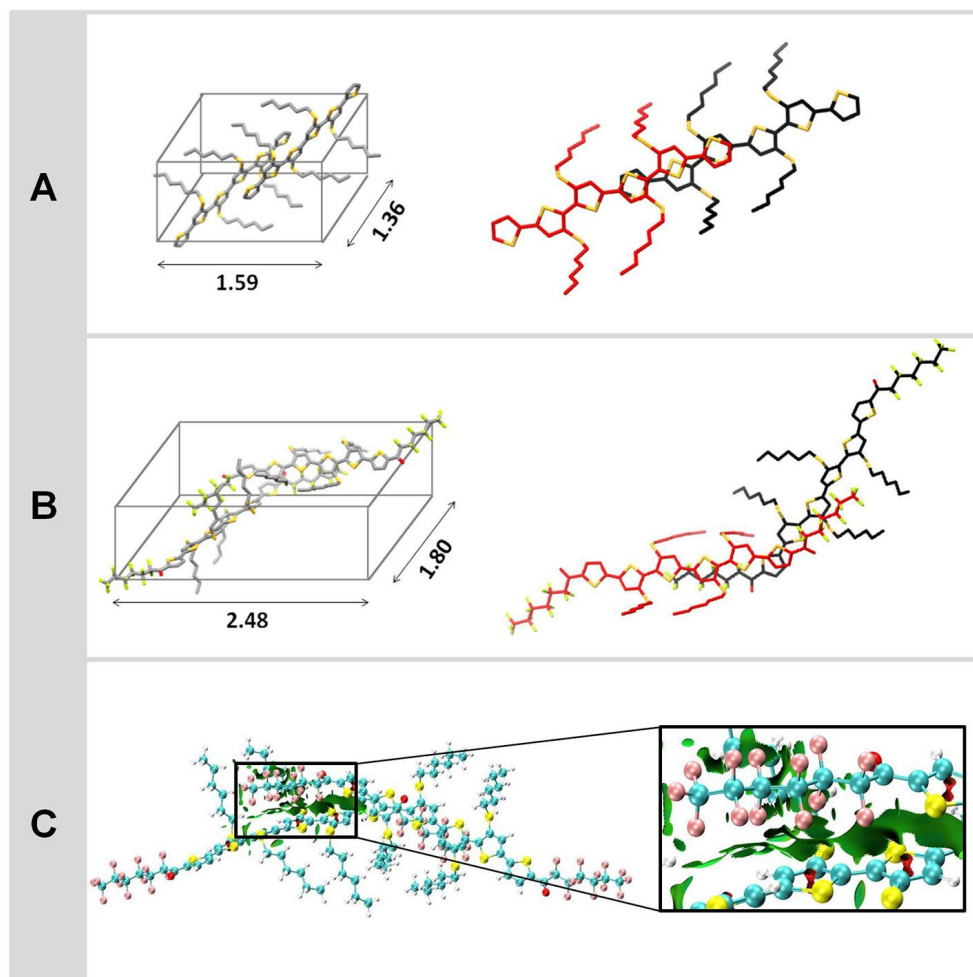

Figure 8. A), B) Sketches of the proposed unit cells of the fibers of **5** and **8** (axes lengths in nm being obtained from the distances of the main reflections of X-ray plots and DFT calculated conformations of the dimers of **5**, **8**. C) NCI (non covalent interaction indicator) isosurface plots for the dimer of compound **8** identifying hydrogen bonding regions (the green regions between the two molecules). For clarity, the isosurfaces were generated only for the regions indicated by the box. Adapted from reference [11b].
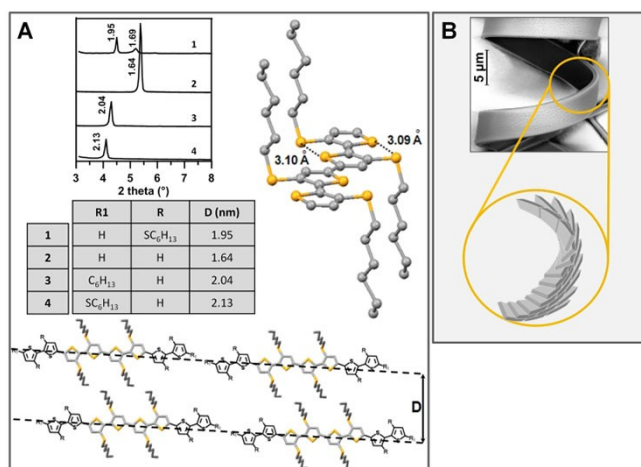
ChemistryOpen

Minireviews
doi.org/10.1002/open.201900347

Chemistry Europe
European Chemical
Societies Publishing

Figure 9. A) X-ray diffraction pattern of the fibers of compounds **1**–**4** grown on glass; periodic distances reported in nm; conformation of the inner tetrameric core of the octamers as determined by single crystal X-ray analysis of compound **2** and model of J-type stacking. B) A detail of the film from **4** and proposed model for the supramolecular packing. Adapted from reference [11a].

crystal X-ray analysis of octamer **2** confirmed our assumptions.[11a,23] The single crystal conformation of the quaterthiophene inner core of **2** is shown in Figure 9A. The core is planar with all the sulfur atoms located on the same plane at S⋯S intramolecular distances below the sum of van der Waals radii. Moreover, the thiophene rings are in the *anti* configuration and the S-Hexyl chains are almost perpendicular to the planar backbone to minimize steric hindrance. The small angle peak appearing in each X-ray profile of Figure 9A indicates the distance (D) between columns of J-stacked molecules, which in turn depends on molecular structure. The presence of substituents at the terminal rings causes molecular distortions and small twist of molecular axes leading to stacking defects during

lamellae formation and growth and to the appearance of helical structures in the long range as indicated in Figure 9B.

Combining powder X-ray diffraction and DFT calculations data, we developed a model for the growth of tape-like and helical fibers of compounds **1**–**9** and their packing mechanism into crystalline structures. Figure 10 illustrates the mechanism suggested for the growth process of the fibers and the chirality transfer from the molecular level to the supramolecular meso and microscale.

According to theoretical calculations, intermolecular interactions, based on π–π stacking and/or H-bonding mediated π–π stacking, cause some interring torsions in the molecular backbone. These molecular torsions, which are at the origin of conformational chirality, are also present inside the unit cell of the crystal. Several coherently aligned unit cells build the crystal domains and each crystal is formed by several domains. The crystalline unit cells assemble together to form platelets that can pack either as tape-like or coiled fibers depending on packing forces. During the growth of the nanocrystals chirality transfer to a larger scale takes place. Regular stacking faults driven by intermolecular interactions cause the formation of elongated helices developing along the growth direction. The fluorinated alkyl chains of **8** have some difficulties to regularly assemble in the crystal and consequently the crystal domains are smaller. The same is true for the crystals that markedly twist and shift during the stacking process and which then grow as more screwed helices.[11b]

9. Summary and Outlook

The latest developments in the field of 1D self-assembled thiophene-based microfibers on surfaces have been summarized. In the last few years the research in this field has progressively shifted from morphology and properties optimization to the attempt to understand and control the self-assembly process itself *via* the synthesis of building blocks
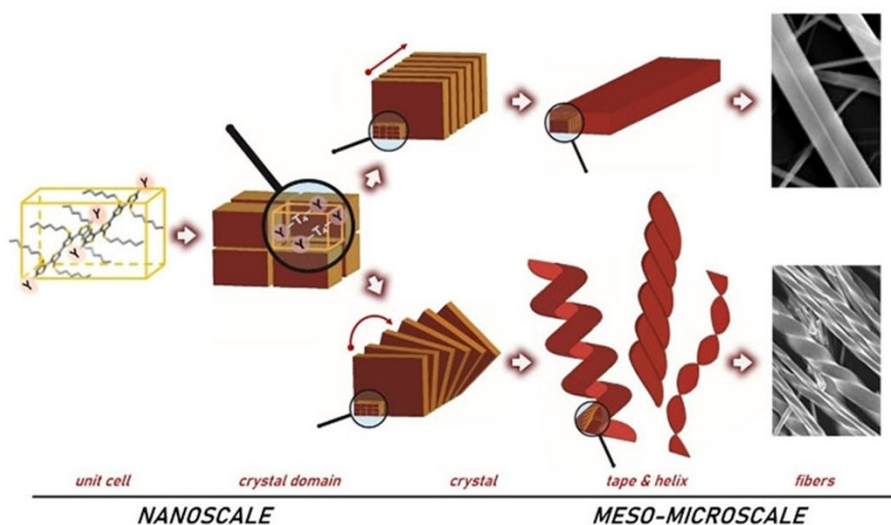

Figure 10. Proposed growth model for the tape-like and helical crystalline fibers of compounds **1**–**9**. Reproduced with permission from reference [11b].

ChemistryOpen

Minireviews
doi.org/10.1002/open.201900347

Chemistry
Europe
European Chemical
Societies Publishing

containing precise structural elements capable to induce the formation of desired supramolecular structures. Oligomers able to undergo significant modifications in their electronic distribution without changing the self-assembly modalities were synthesized and a set of structurally comparable series of microfibers was obtained displaying a wide tuning of optical properties, redox potentials, photoconductivity, and type of prevailing charge carriers (from p- to n-type). Achiral building blocks generated tape-like as well as helical microfibers, all displaying chirality at the nanoscale as demonstrated by circular dichroism signals. It was found that the microfibers were reproducibly obtained on a variety of different surfaces including the SiO$_2$ surface of a field-effect transistor with gold contacts, suggesting that the microfibers could also be directly deposited as electrical circuit components. Hopefully, the results achieved and the knowledge acquired so far will allow to design and synthesize more efficient materials and develop new concepts and ideas for future research and application in the field of semiconducting organic materials.

Acknowledgements

Conflict of Interest

The authors declare no conflict of interest.

[1] a) K. Xu, S. Xie, *Instrum. Sci. Technol.* **2019**. https://doi.org/10.1080/10739149.2019.1660182; b) C. L. Chochos, M. Spanos, A. Katsouras, E. Tatsi, S. Drakopoulou, V. G. Gregoriou, A. Avgeropoulos, *Prog. Polym. Sci.* **2019**, *91*, 51–79; c) H. Ouchi, X. Lin, S. Yagai, *Chem. Lett.* **2019**, *48*, 1009–1018; d) V. Vohra, T. Anzai. *J. Nanomater.* **2017**, vol. 2017, Article ID 3624750, 18 pages. https://doi.org/10.1155/2017/3624750; e) A. Wang, W. Shi, J. Huang, Y. Yan, *Soft Matter* **2016**, *12*, 337–357.

[2] K. Ariga, S. Watanabe, T. Mori, J. Takeya, *NPG Asia Mater.* **2018**, *10*, 90–106.

[3] X. Wang, W. Peng, C. Pan, Z. L. Wang, *Semicond. Sci. Technol.* **2017**, *32*, 043005 (16pp).

[4] a) Y. Wu, Y. Peng, H. Bohra, J. Zou, V. D. Ranjan, Y. Zhang, Q. Zhang, M. Wang, *ACS Appl. Mater. Interfaces* **2019**, *11*, 4833–4841; b) M. A. Doucey, S. Carrara, *Trends Biotechnol.* **2019**, *37*, 86–99; c) F. Di Maria, E. Zucchetti, F. Lodola, F. Benfenati, G. Lanzani, *Chem. Soc. Rev.*, **2018**, 47, 4757–4780.

[5] a) G. Barbarella, M. Zangoli, F. Di Maria, in *Adv. Heterocycl. Chem. Vol. 123* (Eds.: E. F. V. Scriven, C. A. Ramsden) **2017**, pp. 105–167; b) *Handbook of Thiophene-Based Materials: Applications in Organic Electronics and Photonics*, (Eds.: I. F. Perepichka, D. Perepichka), Wiley, **2009**.

[6] a) F. Bastianini, G. E. Pérez, A. R. Hobson, S. E. Rogers, A. J. Parnell, M. Grell, A. Flores Gutiérrez, A. D. F. Dunbar, *Sol. Energ. Mat. Sol. C.* **2019**, *202*, 110128; b) L. Janovák, Á. Dernovics, L. Mérai, Á. Deák, D. Sebők, E. Csapó, A. Varga, I. Dékányab, C. Janáky, *Chem. Commun.* **2018**, *54*, 650–653; c) R. Marty, R. Szilluweit, A. Sánchez-Ferrer, S. Bolisetty, J. Adamcik,

R. Mezzenga, E. C. Spitzner, M. Feifer, S. N. Steinmann, C. Corminboeuf, H. Frauenrath, *ACS Nano* **2013**, *7*, 8498–8508; d) Z. Guo, Y. Wang, X. Zhang, R. Gong, Y. Mu, X. Wan, *Front. Chem.* **2019**, *7*, Article 467.

[7] X. Xing, Q. Zeng, M. Vagin, M. Fahlman, F. Zhang, *Nano Energy* **2018**, *47*, 123–129.

[8] G. Barbarella, F. Di Maria, *Acc. Chem. Res.* **2015**, *48*, 2230–2241.

[9] M. L. Navacchia, L. Favaretto, E. Treossi, V. Palermo, G. Barbarella, *Macromol. Rapid Commun.* **2010**, *31*, 351–355.

[10] J. M. Lehn, *Angew. Chem. Int. Ed.* **2015**, *54*, 3276–3289; *Angew. Chem.* **2015**, *127*, 3326–3340.

[11] a) F. Di Maria, P. Olivelli, M. Gazzano, A. Zanelli, M. Biasiucci, G. Gigli, D. Gentili, P. D'Angelo, M. Cavallini, G. Barbarella, *J. Am. Chem. Soc.* **2011**, *133*, 8654–8661; b) F. Di Maria, M. Zangoli, M. Gazzano, E. Fabiano, D. Gentili, A. Zanelli, A. Fermi, G. Bergamini, D. Bonifazi, A. Perinot, M. Caironi, R. Mazzaro, V. Morandi, G. Gigli, A. Liscio, G. Barbarella, *Adv. Funct. Mater.* **2018**, *28*, 1801946.

[12] Zangoli, Mattia (**2018**), *Property tuning and supramolecular organization of oligo- and polythiophenes for applications in biology and organic electronics*, [Dissertation thesis], Alma Mater Studiorum Università di Bologna, Dottorato di ricerca in Chimica http://amsdottorato.unibo.it/view/dottorati/DOT498/, 30 Ciclo. DOI 10.6092/unibo/amsdottorato/8382.

[13] D. H. Kim, D. Y. Lee, H. S. Lee, W. H. Lee, Y. H. Kim, J. I. Han, K. Cho, *Adv. Mater.* **2007**, *19*, 678–682.

[14] a) M. Surin, P. Leclère, S. De Feyter, M. M. S. Abdel-Mottaleb, F. C. DeSchrywer, O. Henze, W. J. Feast, R. Lazzaroni, *J. Phys. Chem. B* **2006**, *110*, 7898–7908; b) F. Balzer, M. Schiek, A. Lutzen, H. G. Rubahn, *Chem. Mater.* **2009**, *21*, 4759–4767.

[15] B. K. An, S. H. Gihm, J. W. Chung, C. R. Park, S. K. Kwon, S. Y. Park, *J. Am. Chem. Soc.* **2009**, *131*, 3950–3957.

[16] F. Di Maria, E. Fabiano, D. Gentili, M. Biasiucci, T. Salzillo, G. Bergamini, M. Gazzano, A. Zanelli, A. Brillante, M. Cavallini, F. Della Sala, G. Gigli, G. Barbarella, *Adv. Funct. Mater.* **2014**, *24*, 4943–4951.

[17] a) P. Leclère, M. Surin, R. Lazzaroni, A. F. M. Kilbinger, O. Henze, P. Jonkheijm, F. Biscarini, M. Cavallini, W. J. Feast, E. W. Meijer, A. P. H. J. Schenning, *J. Mater. Chem.* **2004**, *14*, 1959–963; b) O. Henze, W. J. Feast, F. Gardebien, P. Jonkheijm, R. Lazzaroni, P. Leclère, E. W. Meijer, A. P. H. J. Schenning, *J. Am. Chem. Soc.* **2006**, *128*, 5923–5929.

[18] a) G. Pescitelli, L. Di Bari, N. Berova, *Chem. Soc. Rev.* **2014**, *43*, 5211–5233.

[19] S. Arias, R. Rodríguez, E. Quiñóá, R. Riguera, F. Freire, *J. Am. Chem. Soc.* **2018**, *140*, 667–674.

[20] a) M. D. Shoulders, R. T. Raines, *Annu. Rev. Biochem.* **2009**, *78*, 929–958; b) M. Hifsudheen, R. K. Mishra, B. Vedhanarayanan, V. K. Praveen, A. Ajayaghosh, *Angew. Chem. Int. Ed.* **2017**, *56*, 12634–12638; *Angew. Chem.* **2017**, *129*, 12808–12812.

[21] R. Berger, H. J. Butt, M. B. Retschke, S. A. L. Weber, *Macromol. Rapid Commun.* **2009**, *30*, 1167–1178.

[22] I. O. Shklyarevskiy, P. Jonkheijm, N. Stutzmann, D. Wasserberg, H. J. Wondergem, P. C. M. Christianen, A. Schenning, D. M. de Leeuw, Z. Tomović, J. S. Wu, K. Müllen, J. C. Maan, *J. Am. Chem. Soc.* **2005**, *127*, 16233–16237.

[23] D. Gentili, F. Di Maria, F. Liscio, L. Ferlauto, F. Leonardi, L. Maini, M. Gazzano, S. Milita, G. Barbarella, M. Cavallini, *J. Mater. Chem.* **2012**, *22*, 20852–20856.

[24] A. Liscio, V. Palermo, P. Samorí, *Acc. Chem. Res.* **2010**, *43*, 541–550.

[25] F. Di Maria, A. Zanelli, A. Liscio, A. Kovtun, E. Salatelli, R. Mazzaro, V. Morandi, G. Bergamini, A. Shaffer, S. Rozen, *ACS Nano* **2017**, *11*, 1991–1999.

[26] L. Yu, *Acc. Chem. Res.* **2010**, *43*, 1257–1266.

[27] a) L. Antolini, G. Horowitz, F. Kouki, F. Garnier, *Adv. Mater.* **1998**, *10*, 382–385; b) T. Siegris, C. Kloc, R. A. Laudise, H. E. Katz, R. C. Haddon, *Adv. Mater.* **1998**, *10*, 379–382.

[28] a) T. Siegris, R. M. Fleming, R. C. Haddon, R. A. Laudise, A. J. Lovinger, H. E. Katz, P. Bridenbaugh, D. D. Davis, *J. Mater. Res.* **1995**, 2170–2173; b) F. Garnier, *Acc. Chem. Res.* **1999**, *32*, 209–215.

[29] a) G. Barbarella, M. Zambianchi, R. Di Toro, M. Colonna, L. Antolini, A. Bongini, *Adv. Mater.* **1996**, *8*, 327–330; b) G. Barbarella, M. Zambianchi, M. Del Fresno, I. Marimon, L. Antolini, A. Bongini, *Adv. Mater.* **1997**, *9*, 484–487.

[30] G. Barbarella, M. Zambianchi, L. Antolini, P. Ostoja, P. Maccagnani, A. Bongini, E. A. Marseglia, E. Tedesco, G. Gigli, G. R. Cingolani, *J. Am. Chem. Soc.* **1999**, *121*, 8920–8926.

[31] I. Viola, F. Della Sala, M. Piacenza, L. Favaretto, M. Gazzano, M. Anni, G. Barbarella, R. Cingolani, G. Gigli, *Adv. Mater.* **2007**, *19*, 1597–1602.

[32] M. Zangoli, M. Gazzano, F. Monti, L. Maini, D. Gentili, A. Liscio, A. Zanelli, E. Salatelli, G. Gigli, M. Baroncini, F. Di Maria, *ACS Appl. Mater. Interfaces* **2019**, *11*, 16864–16871.

[33] *Curr. Chem. Supramolecular Chirality* (Eds: M. Crego-Calama, D. N. Reinhoud), Vol. 265, Springer, Berlin, **2006**.

[34] a) E. R. Johnson, S. Keinan, P. Mori-Sanchez, J. Contreras-Garcia, A. J. Cohen, W. Yang, *J. Am. Chem. Soc.* **2010**, *132*, 6498–6506; b) J. Contreras-Garcia, W. Yang, E. R. Johnson, *J. Phys. Chem. A* **2011**, *115*, 12983–12990; c) J. Contreras-Garcia, E. R. Johnson, S. Keinan, R. Chaudret, J. P. Piquemal, D. N. Beratan, W. Yang, *J. Chem. Theory Comput.* **2011**, *7*, 625–632.